Applied Physics A (2023) 129:566
https://doi.org/10.1007/s00339-023-06825-5

Applied Physics A
Materials Science & Processing

Magnetic fluid hyperthermia controlled by frequency counter and colorimetric program systems based on magnetic nanoparticles

Shehab Elbeltagi[1] · Ahmad M. Saeedi[2] · Maha A. Ali[3] · Samaa I. El-Dek[4]

Received: 24 October 2022 / Accepted: 1 July 2023 / Published online: 22 July 2023

Abstract
Magnetic nanoparticles (MNP) are anticipated to perform better in terms of thermal conductivity when exposed to alternating magnetic fields (AMF). Herein, key parameters for efficient heating are examined in an AMF that is organized and managed by a zero voltage switching (ZVS) and frequency counter system, which has shown great potential for hyperthermia (HT). The present study investigates the set-up of a matched coil coupled with direct current (DC) power and a frequency counter. The set-up technique for inducing HT in magnetic fluid NPs used in in vitro experiments and magnetic fluid calorimetric applications is advanced. Superparamagnetic iron oxide nanoparticles Fe_3O_4 (SPIONs) was prepared by the sonochemical method and coated with polyethylene glycol (Fe_3O_4@PEG). Our sample Fe_3O_4@PEG crystallized nano-size with an average particle size of 14 nm, and high magnetic saturation (M_S) about 49 emu/g. The MNPs exposed to AMF at 300 kHz exhibited the highest thermal values (42–45 °C). The specific absorption rate values of 188, 217, and 234 W/g for the NP concentrations of 5, 10, and 20 mg/ml, respectively reveal the improvement of our set-up to enhance the SPIONs as a thermal agent.

Keywords Zero voltage switching (ZVS) · Frequency counter · MNPs · Thermal camera · And hyperthermia

1 Introduction

The phenomenon of magnetic hyperthermia (MHT), which happens when magnetic nanoparticles (MNP) are targeted to an alternating magnetic field (AMF), is one new and exciting use of MHT [1]. The HT is produced by MNP-mediated conversion of the AMF energy into induction heating, which may be fruitful in some categories of cancers due to the targeted thermal extermination of tumor cells with minor collateral destruction. Furthermore, HT is regarded as a non-invasive treatment for oncological pathologies in which carcinoma and healthy cells of living tissues are triggered to cell damage, necrosis, and apoptosis [2–4]. High-frequency hyperthermia (HFHT), including microwave-HT, radiofrequency-HT, and with radiation or chemotherapy [5], is frequently used as treatment for sophisticated cancers in many nations. Superparamagnetic iron oxide nanoparticles Fe_3O_4 (SPIONs) have major role in important applications in biomedicine, activated by AMF that is employed in targeting certain areas of the human body used in magneto-thermal, MHT and drug delivery. A recent study revealed a huge potential for this technique to manipulate fluid viscosity under flowing conditions, which might be employed by many sectors in addition to the well-known medical uses [6].

SPIONs coated with polyethylene glycol (PEG) exhibit favorable intrinsic physic-chemical properties, high hydrophilicity and flexibility, low immunogenicity and toxicity, and adjustable superior magnetic characteristics [7–10], making them suitable for theranostic and HT agents. The utilization of NPs as well as the intensities of both applied laser and external MF may be reduced if they are concentrated in the tumor location rather than the surrounding area. Neel and Brownian relaxation cause heat to be produced primarily when MF is exposed to external AMF in the MHT technique [11, 12]. MNP-based HT therapy has gained much

✉ Shehab Elbeltagi
shehab_bio@sci.nvu.edu.eg; dr.shehabbiophd@gmail.com

1 Medical Biophysics, Physics Department, Faculty of Science, New Valley University, El-Kharga 72511, New Valley, Egypt

2 Department of Physics, Faculty of Applied Science, Umm AL-Qura University, Makkah 24382, Saudi Arabia

3 Biophysics Department, Faculty of Science, Cairo University, Giza, Egypt

4 Materials Science and Nanotechnology Department, Faculty of Postgraduate Studies for Advanced Sciences, Beni-Suef University, Beni-Suef, Egypt

attention due to its capacity to target and heat inactivate bacterial pathogens and cancer cells in a minimally invasive manner [13, 14]. According to the data, cancer cells are more sensitive to temperatures exceeding 41 °C than normal cells, another emerging treatment for malignant cancer [15, 16] involves the removal of cancer cells at optimal heating between 41 and 46 °C using thermal energy released by MNPs under external AMF.

1.1 Specific absorption rate (SAR)

SAR calculates the MNPs capacity to absorb AMF energy and produce heat energy. It typically refers to the conversion of magnetic energy into HT [17]. SAR technique is the rate at which electromagnetic radiation (or RF) is absorbed by the biological substance per mass unit, is the primary factor regulating tissue heating. It is proportional to the temperature rate increase ($\Delta T/\Delta t$) and is measured in watts per kilo gram in Eq. (1):

$$\mathrm{SAR} = C_{\mathrm{e}}\left(\frac{\Delta T}{\Delta t}\right)\left(\frac{m_{\mathrm{s}}}{m_{\mathrm{m}}}\right)\ldots \tag{1}$$

where C_{e} is the capacity of specific heat suspension equal to 4.186 J/g, m_{s} is the mass of suspension, m_{m} is the mass of the magnetic material in suspension, and $\Delta T/\Delta t$ is the beginning slope of the thermal-time plot in the linear zone [18, 19].

1.2 Application of Arduino microcontroller

Arduino microcontroller is a type of embedded integrated circuit on a straightforward board with a configuration for open-source development that enables computers to direct initiatives that are both artistic and practical. The firmware and essential programming language used by Arduino are stored on the chip. However, it's feasible for non-experts without any programming knowledge to adopt and use the Arduino boards. Arduino shingle technology software and hardware [20], which have this as their main advantage.

In this paper, we investigate the implementation of a newly designed system that uses a set-up connected to an Arduino program to display the magnetic field range in the solenoid copper coil. The high-frequency rate is displayed on the lab top to improve the magnetic HT applications. Apply AMF to magnetic fluid based on MNPs that have high M_S with different concentrations to enhance the SAR values. The present study of the program system that improves the HT rate helps to realize the required SAR values, although the setup computed via the Arduino microcontroller program will help the scientific researchers use it in the future to apply the magnetic HT in both in-vitro and in-vivo magnetic fluid calorimetric approaches.

2 Materials and methods

2.1 Synthesize of superparamagnetic NPs

The preparation of SPIONs coated with polyethylene glycol Fe_3O_4@PEG was carried out by the sonochemical method as reported in our previous work [21].

2.2 Hardware and software for HT set-up

Set-up and loop components make form the basic programming structure for the Arduino microcontroller, it was chosen because it is widely available and circulated, simple to program and control, and inexpensive. All variables needed to set the pin mode or serial communication are stated and defined in the setup components. The Arduino board is changed, responded to, and controlled by the loop components, allowing the coded script to interact [18]. In addition to analogue inputs, the Arduino features fourteen digital I/O pins: A 16 MHz crystal oscillator; the ability to power the Arduino Uno through USB or an external power source (9-V battery); and the ability to configure pin 3 of the serial header in-circuit. Through the modifying, responding, and controlling of the Arduino board, the loop combination enables the coded script to relate to one another [22]. The input for frequency is connected to digitalRead (pin 5) and tracked to the input (16-bit) hardware counter1's alternate port function (T1). More counter overflows are counted and calculated as the resolution is increased, adding the counter value to the long integer result at the end. A single transistor or a 74HC14 inverter, for example, can be used to amplify weak signals if the frequency source (coil) output is digitally leveled. Approximately 8 MHz is the maximum input frequency when the signal duty cycle is 50%. In the start digitalRead () function, the gate time for the counting period can be selected. Values of 10, 100, or 1000 mS are workable for a resolution of 100, 10, or 1 Hz, but any value may be used. The wiring script that was installed on the Arduino Uno used in all of the experimental tests is shown in Fig. 1.

2.3 Set-up and AMF hyperthermia

It is set to a high frequency and operates at a voltage of DC 24–36 V with a current of 15–30 A, for example, in a 24 V 350 W switching power supply. The manufacturer of ZVS is (Aihaozhe Elec, Hong Kong, China) it's cooled by a circulating cooling water pump and connected by a copper coil that has seven turns of an inner diameter of 3.8 cm. The MF creation inside the solenoid coil using a digital DC power supply running at 24 V and 14 amps, and the frequency range of 300 kHz. An oscilloscope was used to adjust and measure

Fig. 1 The set-up program script

```
File  Edit  Sketch  Tools  Help

RF_hyper_thiermia

#include <FreqCounter.h>
#include <LiquidCrystal.h>
// initialize the library with the numbers of the interface pins
LiquidCrystal lcd(7, 8, 9, 10, 11, 12);
void setup() {
  lcd.begin(16, 2);
  //Serial.begin(57600);                    // connect to the serial port
  Serial.println("Frequency Counter");
  lcd.setCursor(0,0);
  lcd.print("RF Hyperthermia");
  lcd.setCursor(0,1);
  lcd.print("Hello Shehab!!!");
  delay(5000);
  lcd.clear();
}
long int frq;
void loop() {
 FreqCounter::f_comp= 8;             // Set compensation to 12
 FreqCounter::start(1000);            // Start counting with gatetime of 1000ms
 while (FreqCounter::f_ready == 0)          // wait until counter ready
  frq=FreqCounter::f_freq;            // read result
 //Serial.println(frq);                // print result
 lcd.setCursor(0,0);
lcd.print("FREQUENCY:");
 lcd.setCursor(0,1);
 lcd.print(frq);
 lcd.print("HZ    ");
delay(20);
 }
```

the output power at a varied frequency from the ZVS circuit. The intensity of the generated MF was detected with a simple magnetometer and compared with the results of the output power of the oscilloscope. The frequency counter developed by the Arduino microcontroller program system and it displays the frequency levels.

2.4 Magnetic induction heating system

Magnetic induction heating set-up with the solenoid coil produces MF within the coil (Fig. 2). The designed solenoid encompasses the full sample volume in a homogeneous field to guarantee reliable readings of SAR [23]. Along with other design features, coil has seven turns made from cylindrical copper plate sections, which improves its performance over a solenoid of a similar size.

MNPs with concentrations (5, 10, and 20 mg/ml) dissolved in 1 ml of ultrapure water was placed in 2.5 mL microcentrifuge tube and fixed by holder inside the center coil without influencing the walls or touching or moving the sample. The rise in sample heating was monitored and recorded every 1 min using Seek thermal cameras with compact heating. An internal water cooling circulation was used to keep coil temperature at room temperature. The following formula, which was derived from (2), was used to calculate magnetic field (H) value in the solenoid coil for MNPs heating ability [24].

$$B = \mu\left[\left(\frac{NI_{\mathrm{rms}}}{2l}\right)\left(\frac{-z+\frac{l}{2}}{\left[\left(z-\frac{l}{2}\right)^2+a^2\right]^{\frac{1}{2}}}+\frac{z+\frac{l}{2}}{\left[\left(z+\frac{l}{2}\right)^2+a^2\right]^{\frac{1}{2}}}\right)\right], \tag{2}$$

where $(\mu)=4\pi 10^{-7}$ (H/m) is free space permeability, (N) is turns number, (L) is coil length, (I_{rms}) is root mean square, and (a) is coil radius.

3 Results and discussion

Surface morphology and transmission electron microscope (TEM).

The morphology and diameter of Fe_3O_4@PEG NPs were measured by using scanning electron microscopy (SEM) at high magnification, SEM scan shown the narrow

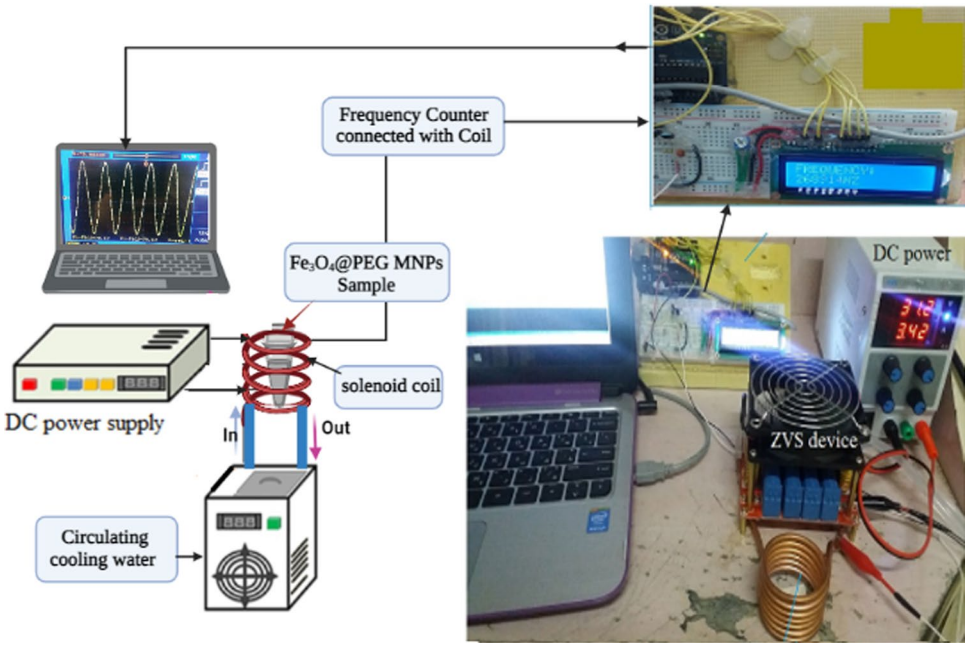

Fig. 2 Block diagram of system device (created in Biorender.com)

size distributed spherical of particles at rang 12 nm (Fig. 3A) as reported in [25]. The Fe_3O_4@PEG sample are approximately spherical and slight agglomeration of primary particles that prepared with Fe_3O_4 to PEG, furthermore, a significant decrease in aggregation between the smaller NPs. Figure 3B explained the TEM image of Fe_3O_4@PEG synthesis appear broad because the crystallite size is too small [21], it is obtained fine SPIONs. Because of their magnetic properties, MNPs contain aggregated NPs average size is 14 nm and geometric shape appears to be cubic.

3.1 Magnetic properties measurements

The magnetic hysteresis loop is clarified in Fig. 3C and Table 1, for the SPIONs under investigation. A small area of Fe_3O_4@PEG exhibits SPIONs behavior as shown by the loops; it is clear that the magnetization saturation (M_S) decreased the smaller size. Due to its extremely tiny size, highest M_S, and good homogeneity, the Fe_3O_4@PEG was shown to be the most beneficial in HT according to the data from the M-H loop [19].

3.2 X-ray diffraction (XRD)

According to Fig. 3D, the XRD charts were indexed and compared to ICDD card 04-015-8207, the Fe_3O_4@PEG crystallized in a cubic spinel structure in a single spinel phase with space group Fd3m. XRD peaks look broad because the crystallite size is too small, and fine SPIONs were produced. The Fe_3O_4@PEG crystallized satisfactorily in cubic spinel form in a single phase without the need for further heat treatment. In the (220), (311), (400), (44 0), and (511) planes, distinct diffraction peaks were seen [21]. So, Bragg inter-planar distance of the crystal and is estimated from diffraction Eq. (3),

$$2d \sin\theta = n\lambda, \tag{3}$$

and the density theoretical was computed from Eq. (4) [26],

$$D_x = \frac{ZM}{NV}, \tag{4}$$

where N is Avogadro's number, Z is the molecules per unit cell number, M is the molecular weight, and V is the unit cell volume ($V = a^3$) in cubic symmetry case. From the Scherrer's Eq. (5) can be calculate the crystallite size (D) because all of the diffraction profiles exhibit broad profile distribution as a result of X-ray scattering from small nanocrystals:

$$D = \frac{k\lambda}{\beta \cos\theta}, \tag{5}$$

where $\lambda = 1.54$ Å, k Scherer constant $= 0.90$ for spherical crystals, and is the corrected full width at half maximum (FWHM) of a peak profile, so the crystallite size was found to be 9.7 nm (Table 1).

3.3 Set-up thermal heating management results

The magnetic heating experiments were carried out using a frequency of 300 kHz, yielding 2.8 mT AMF ($H_F = 0.9 \times 10^9$ Am^{-1} Hz) [27–29]. The set-up is calibrated in the biotechnology department compared to a standard device and

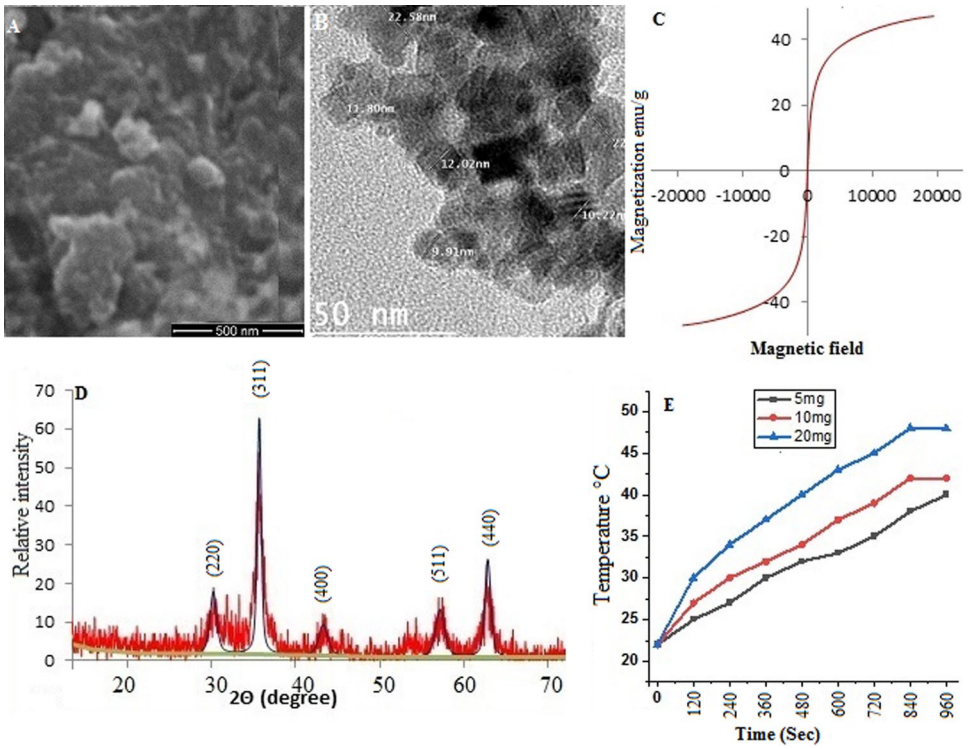

Fig. 3 **A**. SEM scan, **B**. TEM, **C**. VSM, **D**. XRD, and **E**. is the characteristic temperature time plot obtained

controlled by a special program. The Arduino IDE was used to upload the code to the board after all the wires had been connected. The copper coil exposes samples to 2D field amplitude fluctuations by providing a uniform MF of HT in a constrained volume inside the coil [30]. The solenoid coil operates with current field strength and is thus qualified for generating a uniform MF within a sizeable portion of the coil when the power is high [31]. This set-up is unusual in HT since it combines these system elements and links for MF and frequency detections [32], and that can be modified for MF calorimetric. The findings showed that the standard inductor geometry utilized for single cell cultures or small animals is the solenoid coil.

3.4 Magnetic induction heating and SAR evaluation

By capturing time-dependent temperature curves from magnetic induction heating experimental observations, the heating effectiveness of Fe_3O_4@PEG was examined for 15 min. Figure 3E displays the time-dependent temperature characteristic curves. Fe_3O_4@PEG NPs fluid was evaluated at concentrations of 5, 10, and 20 mg/mL, and its capacity for induction heating was investigated at a frequency of 250–300 kHz. Once heat creation and heat loss to the environment by the NPs are balanced, the temperature of the NPs rises quickly at first, then gradually, and finally reaches a maximum [33]. The HT of the MNPs was discovered to be highly reliant on the MNP content, magnetic characteristics, and setup MF. Figure 4A displays the thermal images of Fe_3O_4@PEG taken by a Seek thermal compact camera with scale. Figure 4B describes the SAR values and evolution of thermal-time for a Fe_3O_4@PEG sample with different concentrations under a MF. SAR is evaluating the heat produced by MNPs under MF, which was calculated using Eq. (1), with the higher heating temperatures at 20 mg/mL (T_S) being 47 °C. SAR values for samples were reported in Table 2 to be 188, 217, and 234 W/g at concentrations of 5, 10, and 20 mg/ml respectively. Figure 4C includes the control samples (solution with and without NPs) for comparison purposes.

Table 3, explain comparison between our SAR results and others scientific reported for MNPs and found that they

Table 1 Magnetization saturation value (M_S), Remanent magnetization, (M_r/M_s), loop area, and D

Sample	M_s (emu/g)	M_r (emu/g)	M_r/M_s	H_c (Oe)	Loop area (erg/g)	D from XRD and from TEM (nm)
Fe_3O_4@PEG	49	0.7	0.006	12.9	3727	9.7 and 5

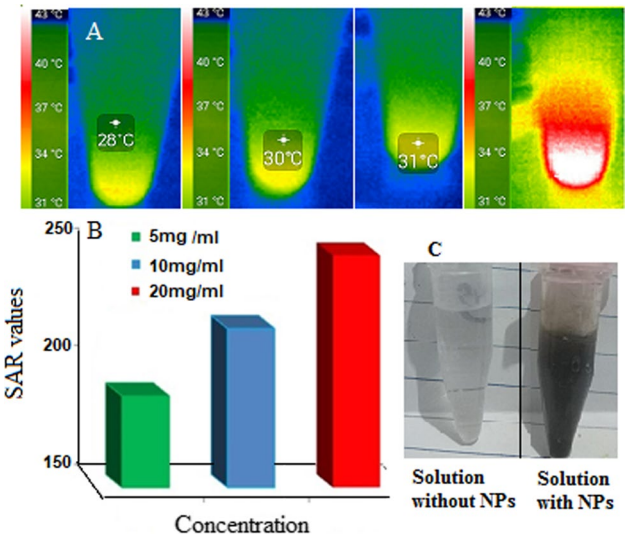

Fig. 4 **A** Thermal images at initial for (20 mg sample) captured at multiple time scales, **B** SAR values, and **C** solution with and without NPs

Table 2 SAR values at various concentrations (5, 10, and 20 mg/ml)

Sample (mg/ml)	M_s.(emu/g)	Particle size (nm)	dT	dT/dt	SAR (W/g)
5 mg	49	14	13.5	0.045	188
10 mg	49	14	20	0.052	217
20 mg	49	14	23	0.056	234

were higher in comparison with Fe_3O_4 colloids suspended in water 15, 0.5 mg at 184, 13.3 kHz, respectively[34, 35]. However, the SAR values are lower than [36] due to multi-core Fe_3O_4, where they used a high current field strength of 26.7 and 38kA/m, respectively. The supplied data in Table 3 made the impressive SAR values apparent [37–39] due to the high-frequency rate, number of turns, high current used, and narrow diameter of copper coil.

The present work uses a new system with a few number of turns with copper coil narrow diameter to get an ideal value for HT that is controlled and computed by a special program. The SAR obtained from MNPs was concluded to be field-amplitude dependent and a critical variable for thermal therapy. Fe_3O_4@PEG NPs at a concentration of 20 mg/ml are evidently promising candidates for their employment as thermal agents in MFH in order to sustain the required range of therapeutic heating for a sufficient amount of time, as shown by the comparison of SAR values [38–43].

4 Conclusion

In this research, in a short period of time, the set-up achieved a high-frequency HT and appropriate SAR values. The high frequency output was computed and developed by the frequency counter Arduino microcontroller program system that able to display the frequency levels and the fluctuations rate inner the coil. The set-up enhanced the measurement of frequency rate and high-frequency hyperthermia (HFHT) using Arduino in the coil and simulations of the MNPs HT. Our system showed a distinguished potential mainly to measure SAR for SPIONs in magnetic fluid calorimetric systems in the future. The set-up can be utilized in medical application tests both in vitro and in vivo based on the concentration, M_S, and crystal size of the NPs are the main parameters controlling their induced magnetic heating.

Table 3 Reported literature on MNPs, coil design, frequency, current, and SAR value

Sample	Concentration (mg/mL)	No. turn of coil	Frequency (kHz)	Current field strength (kA/m)	SAR W/g	References
Fe_3O_4	15	4.5	184	12	12	[34]
Fe_3O_4	0.5	10	13.3 k	–	169	[35]
$Me_{0.4}Zn_0.6Fe_2O_4$	2–10	4/6	265	26.7	334.5	[36]
Fe_3O_4	–	air-coil	50–1000	24	8–595	[37]
$CoFe_2O_4/SiO_2$	10.9	3	180	35 mT	7.22	[38]
Fe_3O_4	100	Single	980	38	100–300	[39]
Fe_3O_4-APTMS	17	3	154	–	25	[40]
Ferro fluid	0.6	9	180	35	–	[41]
Magnetite (Fe_3O_4)	5.8%	–	470–1020	0.1–1.19	208.7	[42]
Fe_3O_4@PEG	5	7	250–300	4	188	Present work
Fe_3O_4@PEG	10	7	250–300	4	217	Present work
Fe_3O_4@PEG	20	7	250–300	4	234	Present work

Author contributions All authors registered have made fundamental, direct, and intellectual contributions to the work discussed in this publication. SE: wrote the paper, made a designed the system and performed the experiments analyzed the data, and AMS, MAA, SIE-D, they drafted and did linguistic revision the paper. All authors discussed the data and revised the manuscript, and also read and approved the final paper manuscript.

Funding Open access funding provided by The Science, Technology & Innovation Funding Authority (STDF) in cooperation with The Egyptian Knowledge Bank (EKB).

Data availability Data of this study are available from the corresponding author on reasonable request.

Declarations

Conflict of interest The authors declare that they have no conflict of interest.

References

1. M.E. Brollo, I.F. Pinheiro, G.S. Bassani, G. Varet, V.C. Guersoni, M. Knobel, A.C. Bannwart, D. Muraca, C. van der Geest, Iron oxide nanoparticles in a dynamic flux: implications for magnetic hyperthermia-controlled fluid viscosity. ACS Appl. Nano Mater. **4**(12), 13633–13642 (2021). https://doi.org/10.1021/acsanm.1c03061
2. M. Suleman, S. Riaz, In silico study of hyperthermia treatment of liver cancer using core-shell $CoFe_2O_4$@$MnFe_2O_4$ magnetic nanoparticles. JJoMM Mater. **498**, 166143 (2020). https://doi.org/10.1016/j.jmmm.2019.166143
3. A. Manohar, D.D. Geleta, C. Krishnamoorthi, J. Lee, Synthesis, characterization and magnetic hyperthermia properties of nearly monodisperse $CoFe_2O_4$ nanoparticles. JCI **46**, 28035–28041 (2020). https://doi.org/10.1016/j.ceramint.2020.07.298
4. I. Ali, Y. Pan, Y. Jamil, A.A. Shah, M. Amir, S. Al-Islam, Y. Fazal, J. Chen, Z. Shen, Comparison of copper-based Cu–Ni and Cu–Fe nanoparticles synthesized via laser ablation for magnetic hyperthermia and antibacterial applications. Physica B **650**, 414503 (2023). https://doi.org/10.1016/j.physb.2022.414503
5. A. Chichet, J. Skowronek, M. Kubaszewska, M. Kanikowski, Hyperthermia—description of a method and a review of clinical applications. Repods Pract. Oncol. Radiother. **5**(12), 267–275 (2007). https://doi.org/10.1016/S1507-1367(10)60065-X
6. F.I. Pinheiro, E.F. Maria-Brollo, S.G. Bassani, G. Varet, D. Merino Garcia, C.B.V. Guersoni, M. Knobel, C.A. Bannwart, D. Muraca, C. van der Geest, Effect of viscosity and colloidal stability on the magnetic hyperthermia of petroleum-based nanofluids. Fuel **331**, 125810 (2023). https://doi.org/10.1016/j.fuel.2022.125810
7. M. Yusefi, K. Shameli, O.S. Yee, S.Y. Teow, Z. Hedayatnasab, H. Jahangirian, T.J. Webster, K. Kuca, Original research highly-accessed green synthesis of Fe_3O_4 nanoparticles stabilized by a garcinia mangostana fruit peel extract for hyperthermia and anticancer activities. Int. J. Nanomed. **16**, 2515–2532 (2021). https://doi.org/10.2147/IJN.S284134
8. Z. Hedayatnas, A. Dabbagh, F. Abnis, W.M.A. Daud, Polycaprolactone-coated superparamagnetic iron oxide nanoparticles for in vitro magnetic hyperthermia therapy of cancer. Eur. Polym. J. **133**, 109789 (2020). https://doi.org/10.1016/j.eurpolymj.2020.109789
9. Z. Hedayatnasab, A. Ramazani, H. Shirgahi, M.R. Mozafari, Heat induction of iron oxide nanoparticles with rational artificial neural network design-based particle swarm optimization for magnetic cancer hyperthermia. Mater. Res. Bull. **157**, 112035 (2023). https://doi.org/10.1016/j.materresbull.2022.112035
10. H. Etemadi, P.G. Plieger, Magnetic fluid hyperthermia based on magnetic nanoparticles: physical characteristics, historical perspective, clinical trials, technological challenges, and recent advances. Adv. Ther. **3**, 200006 (2020). https://doi.org/10.1002/adtp.202000061
11. N. Ajinkya, X. Yu, P. Kaithal, H. Luo, P. Somani, S. Ramakrishna, Magnetic iron oxide nanoparticle (IONP) synthesis to applications: present and future. JM **13**, 4644 (2020). https://doi.org/10.3390/ma13204644
12. I. Ali, Y. Pan, Y. Jamil, A.A. Shah, M. Amir, S.A. Islam, Y. Fazal, J. Chen, Z. Shen, Comparison of copper-based Cu–Ni and Cu–Fe nanoparticles synthesized via laser ablation for magnetic hyperthermia and antibacterial applications. Physica B **650**, 414503 (2023). https://doi.org/10.1016/j.physb.2022.414503
13. I. Raouf, J. Lee, H.S. Kim, M.H. Kim, Parametric investigations of magnetic nanoparticles hyperthermia in ferrofluid using finite element analysis. Int. J. Therm. Sci. **159**, 106604 (2021). https://doi.org/10.1016/j.ijthermalsci.2020.106604
14. G.P. Skandalakis, D.R. Rivera, C.D. Rizea, A. Bouras, J.G. Jesu Raj, D. Bozec, C.G. Hadjipanayis, Hyperthermia treatment advances for brain tumors. Int. J. Hyperth. **37**, 3–19 (2020). https://doi.org/10.1080/02656736.2020.1772512
15. H. Ghayour, M. Abdellahi, N. Ozada, S. Jabbrzare, A. Khandan, Hyperthermia application of zinc doped nickel ferrite nanoparticles. JJoPCo Solids **111**, 464–472 (2017). https://doi.org/10.1016/j.jpcs.2017.08.018
16. S. Nasrin, F.U.Z. Chowdhury, S. Hoque, Study of hydrodynamic size distribution and hyperthermia temperature of chitosan encapsulated zinc-substituted manganese nanoferrites suspension. JPBCM **561**, 54–63 (2019). https://doi.org/10.1016/j.physb.2019.02.053
17. A. Vincent Balogun, B.O. Otanocha, I. Bankole, Development of smart linear velocity measuring device by embedding sensors with the arduino microcontroller. In IML '17 Proceedings of the 1st International Conference on IoT and Machine Learning (2017). https://doi.org/10.1145/3109761.3158399
18. Q. Zeng, I. Baker, J.A. Loudis, Y. Liao, P.J. Hoopes, J.B. Weaver, Weaver, Fe/Fe oxide nanocomposite particles with large specific absorption rate for hyperthermia. Appl. Phys. Lett. **90**, 233112 (2007). https://doi.org/10.1063/1.2746064
19. B. Van, L.W. Bartels, D.A. Leeuw, J.J. Lagendijk, J.B. Van, Experimental validation of hyperthermia SAR treatment planning using MR B1 imaging. Phys. Med. Biol. **22**, 5029–5042 (2004). https://doi.org/10.1088/0031-9155/49/22/001
20. M. Yusefi, K. Shameli, Z. Hedayatnasab, S.Y. Teow, U.N. Ismail, C.A. Azlan, R.R. Ali, Green synthesis of Fe_3O_4 nanoparticles for hyperthermia, magnetic resonance imaging and 5-fluorouracil carrier in potential colorectal cancer treatment. Res. Chem.

Intermed. **47**, 1789–1808 (2021). https://doi.org/10.1007/s11164-020-04388-1
21. S.I. El-Dek, A.A. Maha, M.E. Sara, E.A. Shehab, Comparative investigations on ferrite nanocomposites for magnetic hyperthermia applications. J. Magn. Magn. Mater. **458**, 147–155 (2018). https://doi.org/10.1016/j.jmmm.02.052
22. D.A. Ausilio, Arduino: a low-cost multipurpose lab equipment. Behav. Res. Methods **44**(2), 305–313 (2012). https://doi.org/10.3758/s13428-011-0163-z
23. E.D. Bordelon, C. Cornejo, G. Cordula, W. Fritz, T. DeWeese, R. Ivkov, Magnetic nanoparticle heating efficiency reveals magneto-structural differences when characterized with wide ranging and high amplitude alternating magnetic fields. J. Appl. Phys. **109**, 124904 (2011)
24. M. Subramanian, A. Miaskowski, G. Pearce, J. Dobson, A coil system for real-time magnetic fluid hyperthermia microscopy studies. Int. J. Hyper. **32**(2), 112–120 (2016). https://doi.org/10.3109/02656736.2015.1104732
25. V. Vinodhini, K. Chintagumpala, Superparamagnetic hyperthermia and cytotoxicity properties of bimagnetic core–shell nanoparticles synthesized by solvothermal reflux method. J. Magn. Magn. Mater. **565**, 170290 (2023). https://doi.org/10.1016/j.jmmm.2022.170290
26. M. Yusefi, K. Shameli, O.S. Yee, S. Teow, Z. Hedayatnasab, H. Jahangirian, J.T. Webster, Green synthesis of Fe_3O_4 nanoparticles stabilized by a *Garcinia mangostana* fruit peel extract for hyperthermia and anticancer activities. Int. J. Nanomed. **16**, 2515–2532 (2021). https://doi.org/10.2147/IJN.S284134
27. A. Rajan, N.K. Sahu, Inductive calorimetric assessment of iron oxide nano-octahedrons for magnetic fluid hyperthermia. Colloids Surf. A Physica Eng. Asp. (2020). https://doi.org/10.1016/j.colsurfa.2020.125210
28. A. Hajalilou, L.P. Ferreira, M.E.M. Jorge, C.P. Reis, M.M. Cruz, Superparamagnetic Ag-Fe_3O_4 composites nanoparticles for magnetic fluid hyperthermia. J. Magn. Magn. Mater. **537**, 168242 (2021). https://doi.org/10.1016/j.jmmm.2021.168242
29. N.N. Liu, P.A. Pyatakov, N.M. Zharkov, Optimization of Zn–Mn ferrite nanoparticles for low frequency hyperthermia: Exploiting the potential of superquadratic field dependence of magnetothermal response. Appl. Phys. Lett. **120**, 102403 (2022). https://doi.org/10.1063/5.0082857
30. V. Nemkov, R. Ruffini, R. Goldstein, J. Jackowski, AMF Life Systems LLC, Auburn Hills, Michigan, USA, T.L. DeWeese, R. Ivkov, Magnetic field generating inductor for cancer hyperthermia research. Int. J. Comp. Math. Electr. Electron. Eng. **30**(5), 1626–1636 (2011). https://doi.org/10.1108/03321641111152784.
31. E.D. Bordelon, C.R. Goldstein, S.V. Nemkov, A. Kumar, K.J. Jackowski, T. DeWeese, R. Ivkov, Modified solenoid coil that efficiently produces high amplitude AC magnetic fields with enhanced uniformity for biomedical applications. IEEE Trans. Magn. **48**, 1 (2012). https://doi.org/10.1109/TMAG.2011.2162527
32. V.A. Baloguna, B.I. Oladapo, A.O.M. Adeoye, J.F. Kayode, S.O. Afolabi, Hysteresis analysis of Thornton (IP6, IP12E and TH5V) magnetic materials through the use of Arduino microcontroller. J. Mater. Res. Technol. (2018). https://doi.org/10.1016/j.jmrt.2017.05.018
33. R.R. Akurati, N.K. Jaladi, S.R. Kurapati, G. Kapusetti, M. Choppadandi, P. Mandal, Preparation, characterization and study of magnetic induction heating of Co–Cu nanoparticles. Mater. Today. Commun. **34**, 104964 (2023). https://doi.org/10.1016/j.mtcomm.2022.104964
34. H. Pham, V. Pham, A. Nguyen, C. Nguyen, H. Do, X. Nguyen, V. Le, Magnetic fluid based on Fe_3O_4 nanoparticles: preparation and hyperthermia application. J. Phys. Conf. Ser. **1**, 187 (2009). https://doi.org/10.1088/1742-6596/187/1/012069
35. M.E. Sadat, P. Ronak, S. Jason, L.B. Sergey, C.E. Rodney, Z. Jiaming, X. Hong, W. Yilong, M.P. Giovanni, B.M. David, S. Donglu, Effect of spatial confinement on magnetic hyperthermia via dipolar interactions in Fe_3O_4 nanoparticles for biomedical applications. Mater. Sci. Eng. C **42**, 52–63 (2014). https://doi.org/10.1016/j.msec.2014.04.064
36. V.M. Khot, A.B. Salunkhe, J.M. Ruso, S.H. Pawar, Improved magnetic induction heating of nanoferrites for hyperthermia applications: correlation with colloidal stability and magneto-structural properties. J. Magn. Magn. Mater. **384**, 335–343 (2015). https://doi.org/10.1016/j.jmmm.2015.03.039
37. E. Garaio, J.M. Collantes, J.A. Garcia, F. Plazaola, S. Mornet, F. Couillaud, O. Sandre, A wide-frequency range AC magnetometer to measure the specific absorption rate in nanoparticles for magnetic hyperthermia. J. Magn. Magn. Mater. (2013). https://doi.org/10.1016/j.jmmm.2013.11.021i
38. H. Koichiro, N. Michihiro, S. Wataru, Y. Toshinobu, M. Hirokazu, O. Shuji, A. Masahiro, M. Toshio, I. Kazunori, Superparamagnetic nanoparticle clusters for cancer theranostics combining magnetic resonance imaging and hyperthermia treatment. Theranostics **3**(6), 366–376 (2013). https://doi.org/10.7150/thno.5860
39. M.E. Cano, R.H. Medina, V.V.A. Fern, P.E. Casillas, Magnetic heating ability of silica-cobalt ferrite nanoparticles. Revista Mexicana de Ingenieria Quimica. **13**(2), 555–561 (2014).
40. F.C. Diego, M.Z. Pedro, M. Marzia, P.M. María, C. Aldo, H. Francisco, M.B. Sánchez, R. Fernández, Effect of nanoclustering and dipolar interactions in heat generation for magnetic hyperthermia. Langmuir Jan. (2016). https://doi.org/10.1021/acs.langmuir.5b03559
41. A. Yosefine, S. Youngjin, O. Junghwan, Controlling the optimum dose of AMPTS functionalized-magnetite nanoparticles for hyperthermia cancer therapy. Appl. Nanosci. **1**, 237–246 (2011). https://doi.org/10.1007/s13204-011-0032-1
42. Z.M. Vanessa, F.G. Mar, G.G. Álvaro, S. Beatriz, S.R. Julio, G. Gerardo, H. Rebeca, M. Carmen, Chitosan nanoparticles for combined drug delivery and magnetichyperthermia: from preparation to in vitro studies. Carbohydr. Polym. **157**, 361–370 (2017). https://doi.org/10.1016/j.carbpol.2016.09.084
43. S. Guba, B. Horváth, I. Szalai, Application and comparison of thermistors and fiber optic temperature sensor reference for ILP measurement of magnetic fluids in double cell magnetic hyperthermia. Heliyon **8**, e09606 (2022). https://doi.org/10.1016/j.heliyon.2022.e09606